Atmospheric-pressure dielectric barrier discharge with capillary injection for gas-phase nanoparticle synthesis

Souvik Ghosh[1], Tianqi Liu[1], Mihai Bilici[1], Jonathan Cole[1], I-Min Huang[1], David Staack[2], Davide Mariotti[3] and R Mohan Sankaran[1]

[1] Case Western Reserve University, Cleveland, Ohio, USA
[2] Texas A&M University, College Station, TX, USA
[3] University of Ulster, Newtonabbey, UK

E-mail: mohan@case.edu

Abstract

We present an atmospheric-pressure dielectric barrier discharge (DBD) reactor for gas-phase nanoparticle synthesis. Nickel nanoparticles are synthesized by homogenous nucleation from nickelocene vapor and characterized online by aerosol mobility measurements. The effects of residence time and precursor concentration on particle growth are studied. We find that narrower distributions of smaller particles are produced by decreasing the precursor concentration, in agreement with vapor nucleation theory, but larger particles and aggregates form at higher gas flow rates where the mean residence time should be reduced, suggesting a cooling effect that leads to enhanced particle nucleation. In comparison, incorporating a capillary gas injector to alter the velocity profile is found to significantly reduce particle size and agglomeration. These results suggest that capillary gas injection is a better approach to decreasing the mean residence time and narrowing the residence time distribution for nanoparticle growth by producing a sharp and narrow velocity profile.

Keywords: dielectric barrier discharge, atmospheric-pressure plasma, nanoparticle, homogeneous nucleation, aerosol

⑤ Online supplementary data available from stacks.iop.org/JPhysD/48/314003/mmedia

(Some figures may appear in colour only in the online journal)

1. Introduction

Since the first observations of particle formation in reactive plasmas, homogeneous nucleation of nanoparticles in plasma processes has been of keen interest for dust mitigation during chemical vapor deposition (CVD) of thin films [1–3]. More recently, plasma systems have been developed to promote and control the formation of nanoparticles for materials applications [4–6]. The non-equilibrium environment present in a low-temperature plasma allows the synthesis of unique nanoparticle materials, such as silicon [7] and diamond-phase carbon [8], at pressures and temperatures far away from their thermodynamic phase equilibrium.

Of particular interest for nanoparticle production is operation at atmospheric pressure which would lower costs and simplify manufacturing [9]. Some of the earliest atmospheric-pressure studies were carried out using thermal plasmas and generating nanoparticles by spark ablation [10], homogenous nucleation [11, 12], and spraying [13]. More recently, non-equilibrium, low-temperature atmospheric-pressure plasmas such as direct-current (dc) microplasmas [14–16] and microwave sources [17] have been reported. However, in comparison to low-pressure, low-temperature plasma systems, atmospheric-pressure, low-temperature plasmas continue to have a major drawback in that the production rate is significantly lower due to the reduced plasma volume.

Scale-up of atmospheric-pressure plasma systems such as dc microplasmas could be achieved by operating the microplasmas in parallel, as an array [18]. Unfortunately, dc microplasmas are difficult to operate in parallel because of negative resistivity, which makes it necessary to ballast [19], and even then, must be precisely engineered to control the current in individual elements. In comparison, dielectric barrier discharges (DBD) are highly scalable atmospheric-pressure plasmas, as demonstrated by their implementation in several industrial applications including ozone generation [20]. However, unlike commercial DBDs that produce ozone at large scales by running in parallel plate geometries, coaxial geometry DBDs are more desirable for nanoparticle synthesis to limit the residence time for particle growth. Coaxial configurations require scale up by fabricating an array and operating in parallel [21] or forming in cross-flow geometries where the plasma volume is scaled perpendicular to the direction of gas flow [22]. To our knowledge, there are very few studies of coaxially configured DBDs for nanoparticle synthesis [23].

Here, we present a study of an atmospheric-pressure DBD for nanoparticle synthesis. In order to control particle nucleation and growth, the DBD electrodes were set up in a coaxial geometry rather than in the more typical parallel plate geometry [20]. We focused on the synthesis of nickel (Ni) nanoparticles from an organometallic precursor, cyclopentadienyl nickel [Ni(Cp)$_2$] or nickelocene, and characterized the particles primarily by aerosol mobility measurements which provide online diagnostics of nanoparticle nucleation and growth. In our original configuration, we found that the mean particle size was large and the particle size distributions (PSDs) were broad which is undesirable for both fundamental study and technological application. Inspired by the dc microplasma configuration [14], we added a metal capillary tube to the DBD reactor to inject gas at a higher velocity through the plasma volume, and found that the mean particle diameter could be significantly reduced with a concomitant narrowing of the PSD. These results could not be replicated by increasing the volumetric flow rate through the DBD reactor to decrease the mean residence time. We explain this effect in terms of the gas velocity distribution, which is shifted from a typical laminar profile to a much narrower and sharper profile by the capillary injection. Thus, the residence time distribution for particle growth is also shifted to a smaller mean residence time with a narrower distribution, without affecting the cooling rate as in the case of increasing the volumetric flow rate. Our study demonstrates that atmospheric-pressure DBDs can be effectively used for the synthesis of nanoparticles if the residence time distribution is controlled as it is here by capillary gas injection.

2. Experimental details

Two basic configurations of a DBD were designed, fabricated, and studied for nanoparticle synthesis, based on a coaxial electrode geometry. The first configuration, schematically shown with accompanying photos of the reactor setup and the DBD operating in figure 1(*a*), consisted of a 6 mm OD × 2 mm ID quartz tube with a powered electrode on the outside and a grounded electrode on the inside (detailed later). We note that a discharge could not be ignited in our background gas, argon (Ar), without having a ground in contact with the gas. The second configuration, schematically shown with accompanying photos of the reactor setup and the DBD operating in figure 1(*b*), consisted of a quartz tube, but with a stainless steel capillary tube on the upstream side of the gas flow to inject gas into the plasma. We studied the injection of the gas using two different size capillary tubes, one with an inner diameter of 510 μm, and another with an inner diameter of 180 μm.

To synthesize Ni nanoparticles, vapors of nickelocene at 25°C (Strem Chemicals) were carried into the reactor by sublimation of a solid powder at room temperature in a flow of Ar. A separate stream of pure Ar was used to dilute and control the final vapor concentration of nickelocene in the DBD (see supporting information, figure S1) (stacks.iop.org/JPhysD/48/314003/mmedia). The final nickelocene vapor concentration was calculated from vapor pressure data [24] and a combination of Dalton's Law and Amagat's Law, using the following formula:

$$y_{\mathrm{Ni}} = \frac{(P_{\mathrm{Ni}}^* / P_{\mathrm{tot}}) \dot{V}_C}{\dot{V}_C + \dot{V}_{\mathrm{Ar}}}$$

where P_{Ni}^* is the vapor pressure of nickelocene at 25 °C, P_{tot} is the reactor inlet pressure which also corresponds to the pressure at the nickelocene source, $\dot{V}_C$ is the volumetric flow rate of Ar carrier gas, and $\dot{V}_{\mathrm{Ar}}$ is the volumetric flow rate of the pure Ar dilution stream. The introduction of the capillary was found to increase P_{tot} significantly, as measured by an inline pressure gauge. A summary of the calculated nickelocene vapor concentrations at the various experimental conditions used in this study are shown in table 1.

The DBD was ignited and operated at steady state by an alternating current (ac) high voltage power supply (Information Unlimited, PVM 500). Copper tape of width 3–4 mm was wrapped around the exterior of the quartz tube such that the upstream edge of the tape aligned with the edge of the capillary tube inside the quartz tube and operated as the powered electrode. The other edge of the tape aligned with a grounded tungsten wire (100 μm diameter, Alfa Aesar) placed inside the quartz tube downstream of the capillary tube, which was also grounded. The applied voltage was measured by a 1000:1 high voltage probe connected directly to the powered electrode and the current was measured by the voltage drop across a resistor in series with the grounded tungsten electrode. For all experiments, a peak-to-peak voltage of ~8 kV at a frequency of 20–30 kHz was applied. The peak-to-peak voltage was found to control the plasma volume, with increasing voltage producing a larger volume plasma (see supporting information, figure S2) (stacks.iop.org/JPhysD/48/314003/mmedia). The current traces exhibited spikes representative of filamentary streamers (see supporting information, figure S3) (stacks.iop.org/JPhysD/48/314003/mmedia). No significant change in the waveforms was observed with and without the capillary tube gas injection. The power consumed by the discharge was estimated to be ~1.0 W with or without the capillary gas
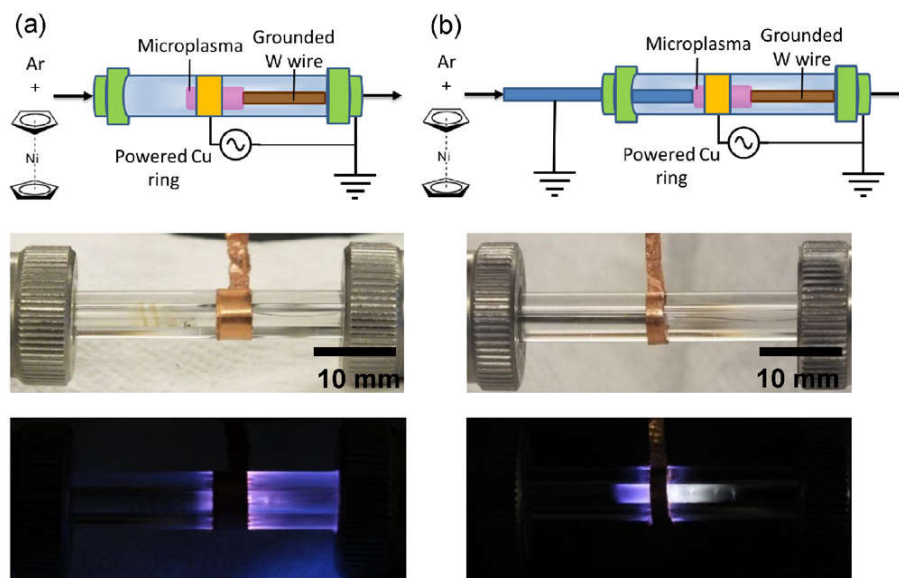
Figure 1. Schematic illustration and photos of atmospheric-pressure DBD reactor setup (*a*) without and (*b*) with 180 μm capillary gas injection.

Table 1. Ar dilution/Ni(Cp)$_2$ carrier (Ar).

Capillary tubes (μm)	Total flowrate (sccm)	Ar/Ni(Cp)$_2$ flowrate (sccm)	Inlet reactor pressure (kPa)	Ni(Cp)$_2$ concentration (ppm)
180	100	95/5	221	0.21
510	100	95/5	104	0.46
No capillary	100	95/5	101	0.47
180	100	90/10	221	0.43
510	100	90/10	105	0.91
No capillary	100	90/10	101	0.94
180	100	80/20	221	0.86
510	100	80/20	104	1.83
No capillary	100	80/20	101	1.88
180	100	70/30	221	1.29
510	100	70/30	104	2.74
No capillary	100	70/30	101	2.81
180	200	180/20	336	0.28
510	200	180/20	106	0.89
No capillary	200	180/20	101	0.94
180	400	360/40	568	0.17
510	400	360/40	111	0.85
No capillary	400	360/40	101	0.94
180	800	720/80	1033	0.09
510	800	720/80	124	0.77
No capillary	800	720/80	101	0.94

injector (see supporting information, figure S4) (stacks.iop.org/JPhysD/48/314003/mmedia).

After introducing the nickelocene vapor, nanoparticle formation was monitored by on line aerosol mobility measurements using a scanning mobility particle sizer (SMPS) spectrometer consisting of a 'Nano' differential mobility analyzer (TSI, Inc., Model 3085) and butanol-based condensation particle counter (TSI, Inc., Model 3776). The lower size limit of detection for the measurements was approximately 2.0 nm. The PSDs approached a steady-state approximately 30 min after the nickelocene was introduced. The steady-state PSDs were then fit to log normal distributions to obtain a geometric mean diameter, D_g, and geometric standard deviation, σ_g.

To support the aerosol measurements of the nanoparticle size, the Ni nanoparticles were also collected for characterization by transmission electron microscopy (TEM). The aerosol leaving the reactor was passed through a 40 μm pore size Teflon filter (Millipore, Inc.) and dispersed in solution by sonicating in 1 mL of isopropyl alcohol for 30–60 s. The dispersions were drop cast onto holey carbon coated copper grids. TEM and energy dispersive spectroscopy (EDX) were performed using a FEI Tecnai F30 with an onboard EDX unit (Oxford Instruments).
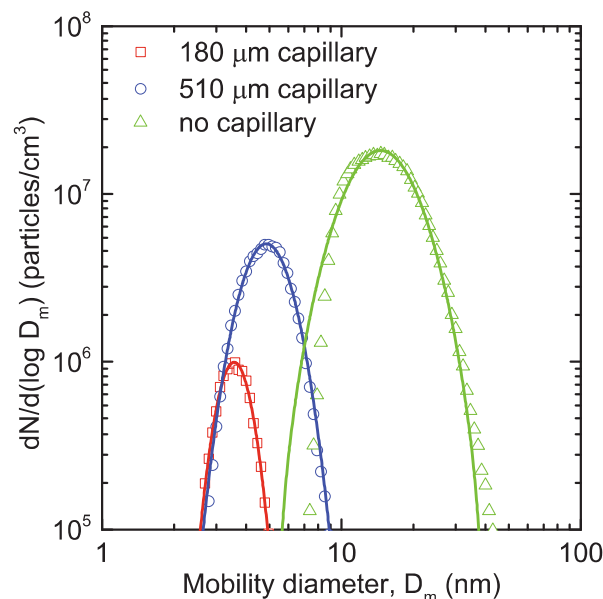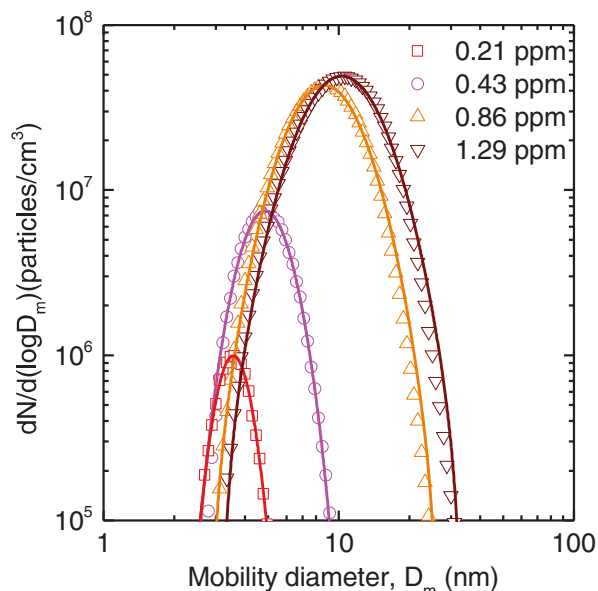
Figure 2. Steady-state aerosol mobility measurements of Ni nanoparticles synthesized in DBD reactor with and without capillary gas injectors (180 μm or 510 μm) at a constant nickelocene carrier gas flow rate of 5 sccm and total gas flow rate of 100 sccm. The precursor flow rate corresponds to 0.21, 0.46, and 0.47 ppm nickelocene in the reactor for the 180 μm capillary, 510 μm capillary, and no capillary cases, respectively.

3. Results and discussion

Aerosol mobility measurements provide an online diagnostic of nanoparticle formation. Here, aerosol mobility measurements are reported under steady-state conditions, defined as when the PSDs remained unchanged for constant process parameters (gas flow rate, precursor concentration, applied power, etc). Since our process is continuous, the steady-state results are an accurate measure of the operation characteristics of the reactor.

Aerosol mobility measurements are based on the electrical mobility of a charged material in the gas phase. The electrical mobility describes the ability of a charged object to move through a viscous medium in an electric field, and for unagglomerated, spherical nanoparticles is directly related to the particle diameter. For other shapes, including fractal aggregates, the electrical mobility is directly related to an aerodynamic diameter, which is not the primary particle diameter, but a characteristic length corresponding to the projected area. Although the measured PSDs may thus not always be representative of the individual particle diameters, with careful interpretation, its shape can give important information about particle size and agglomeration. Because of this ambiguity, the raw data from mobility measurements is shown as the mobility diameter, D_m, and two parameters are extracted from log-normal fits to the PSDs, D_g and σ_g, as characteristic features of the distributions.

Figure 2 shows steady-state aerosol mobility measurements of Ni nanoparticles synthesized in the atmospheric-pressure DBD with and without a capillary gas injector. In

Figure 3. Steady-state aerosol mobility measurements of Ni nanoparticles synthesized in the DBD reactor with a 180 μm capillary gas injector at a total gas flow rate of 100 sccm as a function of nickelocene precursor concentration.

the case of a capillary gas injector, tubes with two different diameter holes were used (510 and 180 μm). The nickelocene carrier and total volumetric flow rates were kept constant in all cases at 5 and 100 sccm, respectively. We note that for the 180 μm capillary tube, the reactor inlet pressure was much higher (see figure S5, supporting information) (stacks.iop.org/JPhysD/48/314003/mmedia), leading to a lower nickelocene vapor concentration (0.21 ppm) than for the experiments with the 510 μm capillary tube (0.46 ppm) and no capillary (0.47 ppm). As we discuss later, the difference in vapor concentrations alone does not explain the large shifts in the mobility diameter. When no capillary gas injector was used, the as-synthesized nanoparticles exhibit a relatively large D_g of 15.0 nm and a broad PSD with a σ_g of 1.35. The large σ_g and shape of the PSD which shows a pronounced tail suggests significant agglomeration. The introduction of a capillary gas injector was found to significantly decrease the mean mobility diameter and narrow the PSD. For a 510 μm capillary gas injector, D_g and σ_g from the aerosol mobility measurements are 4.8 nm and 1.24, respectively, and for a 180 μm capillary gas injector, are 3.7 nm and 1.16, respectively. These values are indicative of unagglomerated spherical nanoparticles and show that the capillary gas injection reduces the particle size and narrows their size distribution.

To address the effect of precursor concentration on nanoparticle nucleation and growth, we synthesized Ni nanoparticles at different nickelocene vapor concentrations. Figure 3 shows steady-state aerosol mobility measurements of Ni nanoparticles synthesized in a DBD with a 180 μm capillary gas injector at a fixed total volumetric flow rate of 100 sccm. The nickelocene vapor concentration in the DBD was controlled by changing the Ar carrier flow rate through the nickelocene precursor with

respect to the pure Ar dilution flow rate. The measured PSDs show that D_g increases from 3.7 nm at 0.21 ppm to 4.9 nm at 0.43 ppm to 8.6 nm at 0.86 ppm to 11.9 nm at 1.29 ppm, with corresponding increases in σ_g from 1.16 to 1.25 to 1.37 to 1.48, respectively. These results indicate that nickelocene vapor concentration also has a strong effect on nanoparticle nucleation and growth, as expected since higher precursor concentrations lead to higher supersaturation and, therefore, increased nucleation of cluster nuclei which can then coagulate and grow into larger particles or aggregate to form agglomerates. However, in comparing the results in figures 2 and 3, precursor concentration alone cannot explain the effect of capillary injection on the PSDs. Firstly, the 510 μm capillary gas injector has a negligible pressure drop and leads to almost no change in the nickelocene vapor concentration as compared to the no capillary scenario (0.46 versus 0.47 ppm), and yet produces smaller nanoparticles with a narrower distribution. Secondly, in the case of the 180 μm capillary injector, although there is a significant pressure drop and decrease in the nickelocene vapor concentration as compared to the no capillary scenario (0.21 versus 0.47 ppm), the shift in particle size and standard deviation of the PSD observed in figure 2 is much larger than that observed in figure 3 for a similar change in nickelocene vapor concentration (compare the PSDs for 0.21 and 0.43 ppm). Therefore, we conclude that capillary injection has an enormous influence on particle growth dynamics in the atmospheric-pressure DBD reactor setup. In comparison, we found that while the tungsten wire was needed to ignite the plasma, it had negligible effect on the particle growth. To assess the importance of the wire, two experiments were performed: 1) we compared the particle growth with the tungsten wire at different positions (at center of the tube versus at the tube wall) and 2) we used two different tungsten wire diameters (100 and 250 μm). In both cases, keeping all other experimental conditions the same, the measured PSDs showed virtually no difference, indicating that the wire did not play a significant role (see supporting information, figures S6 and S7) (stacks.iop.org/JPhysD/48/314003/mmedia).

The role of capillary injection on nanoparticle nucleation and growth in the DBD reactor may be highly complicated. A simple explanation for the observed differences is that the introduction of the capillary increases the gas flow velocity and narrows the velocity distribution in the plasma region, which in turn alters the residence time distribution for nanoparticle growth. We hypothesized that a similar result could be obtained by changing the volumetric flow rate through the DBD, which should similarly change the average residence time, assuming no change in plasma volume. Figures 4(*a*) and (*b*) show steady-state aerosol mobility measurements for Ni nanoparticles synthesized with a 510 μm capillary injector and without any capillary, respectively, at varying total volumetric flow rates. The ratio of Ar carrier flow rate to Ar dilution was kept constant in all experiments, but because of a small pressure increase at the source with the 510 μm capillary injector, the nickelocene vapor concentration decreased from 0.91 ppm at 100 sccm to 0.77 ppm at 800 sccm. The vapor concentration remained constant at 0.94 ppm in the case of no capillary. We assumed that the small changes in nickelocene vapor
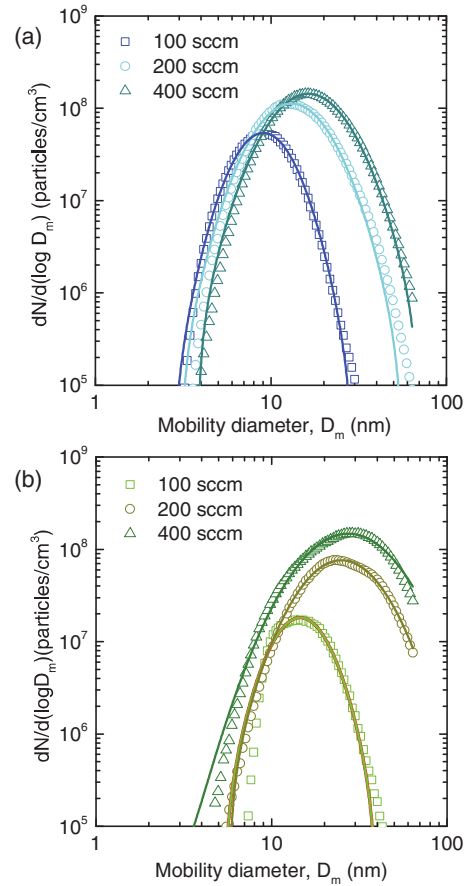
Figure 4. Steady-state aerosol mobility measurements of Ni nanoparticles synthesized in DBD reactor as a function of total gas flow rate (*a*) with a 510 μm capillary gas injector and (*b*) without a capillary gas injector.

concentration had a negligible effect on our interpretation of the results. We also did not carry out these experiments with the 180 μm capillary injector because of the even larger pressure increase at the source associated with this tube diameter. The PSDs show that as the total volumetric flow rate increases, D_g and σ_g increase. In fact, the particle concentrations when the flow rate is increased to >200 sccm are one to two orders of magnitude higher than at 100 sccm, indicating significant nanoparticle nucleation, growth, and agglomeration. These results are contradictory to our picture that as the total flow rate is increased, the average residence time decreases, which should reduce the particle size. We instead interpret these results as the following: as the total volumetric flow rate increases, convective cooling of the plasma is enhanced. Modeling by Girshick *et al* has shown that the cooling rate has a strong effect on nanoparticle nucleation, with higher cooling rates leading to increased nucleation at a given precursor concentration [11]. At the high volumetric flow rates, the nucleation of an increased number of cluster nuclei could then lead to increased growth, resulting in PSDs with a larger D_g and σ_g. Importantly, we point out that increasing the volumetric flow rate did not reproduce the results from the capillary injector and is, therefore, fundamentally different.

J. Phys. D: Appl. Phys. **48** (2015) 314003

S Ghosh *et al*
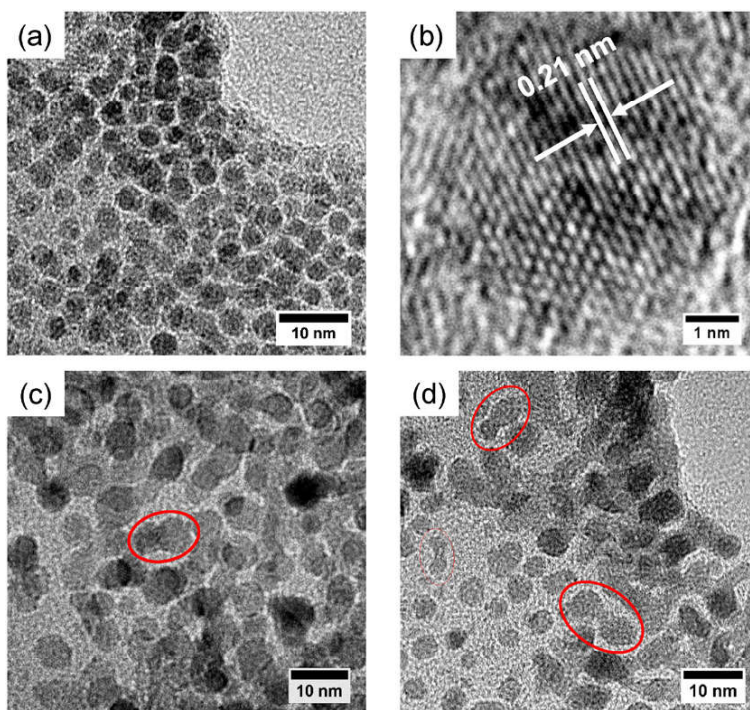
Figure 5. Representative TEM images of Ni nanoparticles synthesized in the DBD reactor (*a*) with a 180 μm capillary gas injector, (*b*) with a 180 μm capillary gas injector at high magnification showing average lattice spacing of 0.21 nm corresponding to Ni(1 1 1), (*c*) with a 510 μm capillary gas injector, and (*d*) without a capillary gas injector. Particle aggregates in (*c*) and (*d*) are indicated by red circles.

We collected the Ni nanoparticles under a selection of growth conditions, particularly with and without the capillary injector, to verify the aerosol mobility results and assess the composition and crystallinity of the material. Figure 5 shows representative TEM images of Ni nanoparticles collected by filtration, dispersed in solution, and drop cast onto substrates. An image of Ni nanoparticles synthesized with a 510 μm capillary injector at a nickelocene vapor concentration of 0.43 ppm and total volumetric flow rate of 100 sccm is shown in figure 5(*a*). The nanoparticles are relatively uniform in size, with an approximate diameter of 5 nm, in agreement with aerosol mobility measurements (see figure 3). The nanoparticles are crystalline, with a measured average lattice spacing of 0.21 nm (see figure S8, supporting information) (stacks. iop.org/JPhysD/48/314003/mmedia), corresponding to the Ni(1 1 1) crystal plane (figure 5(*b*)). From TEM, we could not assess the presence of carbon, which could have been incorporated in the nanoparticle product from the organometallic precursor, since the TEM substrates themselves are made up of amorphous carbon. Previously, we have shown that for dc microplasmas, carbon contamination can be characterized by x-ray photoelectron spectroscopy (XPS) and correlates to the formation of the C_2 Swan band detected by optical emission spectroscopy (OES) [25]. We did not observe any C_2 Swan band in the OES spectra collected from the DBD microplasma, suggesting that solid carbonaceous species were not present in our grown material (see supporting information, figure S9) (stacks.iop.org/JPhysD/48/314003/mmedia). An image of Ni nanoparticles synthesized without a capillary at the same nickelocene vapor concentration and total

volumetric flow rate of 100 sccm is shown in figure 5(*c*). The nanoparticles are found to be larger in size, with an approximate diameter of 8 nm, and slightly agglomerated, which is mostly consistent with aerosol mobility measurements (see figure 4(*a*)). An image of Ni nanoparticles synthesized without a capillary at the same nickelocene vapor concentration and total volumetric flow rate of 800 sccm is shown in figure 5(*d*). In this case, the nanoparticles are found to be approximately 5–10 nm in diameter, and there is significant agglomeration. The particle size is significantly smaller than that measured by aerosol mobility measurements, which indicated ~50 nm; this is most probably because the particles were measured in the gas phase as aggregates and then partially broken up by sonication during preparation of the TEM grid samples. Some aggregates still remain, and overall, this confirms that without a capillary, there is more agglomeration, particularly at the higher gas flow rates. We note that the crystallinity of the synthesized particles does not appear to be affected by the method of precursor injection, as all samples exhibit lattice fringes, although particle imaging is more difficult for samples prepared with a 510 μm capillary or without a capillary because of the agglomeration (see figure S10, supporting information) (stacks.iop.org/JPhysD/48/314003/mmedia). The formation of crystalline particles in a DBD, which is typically characterized by a relatively low gas temperature, may be related to particle heating via interactions with plasma species, as has been previously shown for silicon nanocrystals by modeling of charging and surface reactions [26, 27].

The nucleation and subsequent growth of nanoparticles in a plasma process is highly complicated. To date, no modeling
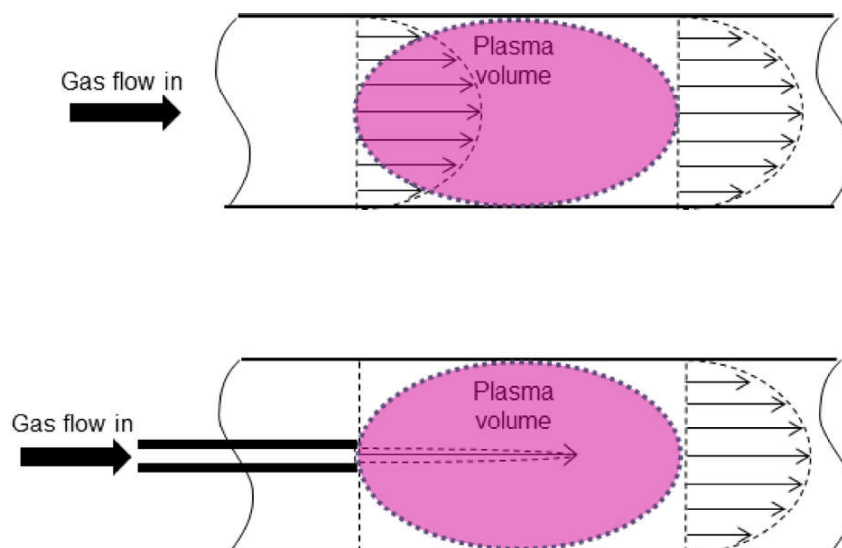
Figure 6. Illustration of conceptualized gas flow velocity distribution in the DBD reactor (*a*) with no capillary and (*b*) with capillary gas injection.

has been carried out on nanoparticle growth dynamics in a non-thermal, atmospheric-pressure plasma system. Theoretical descriptions of vapor phase nucleation have been reported that can provide a qualitative picture of what could be happening in our DBD-based process [11, 28]. In general, particle nucleation occurs by precursor dissociation and radical polymerization, which form initial cluster nuclei at supersaturation conditions. The particles then grow by Brownian coagulation as they are convected through the plasma volume, and as the precursor and radical concentrations decrease. Cluster growth by vapor condensation may also occur, but this is not likely, as the precursor and radical concentrations are rapidly depleted to form the cluster nuclei. Coagulation, which describes the coalescence of particle nuclei into larger clusters, or nanoparticles, is more likely the dominant process. In a plasma, nanoparticles are most probably charged, either by ion or electron attachment or by forming from charged nuclei, which could also contribute electrostatic forces to the coagulation process. As the nanoparticles continue to flow through the plasma volume, agglomeration, which refers to particles colliding and forming aggregates where the primary particles are intact, competes with coagulation. As described in detail by Flagan *et al*, two important process parameters that control the final nanoparticle size are the precursor concentration and the residence time [28]. Our results for the increase in particle size (mobility diameter) with precursor concentration (see figure 3) is completely consistent and confirms that an increase in the supersaturation concentration leads to more cluster nuclei that grow by both coagulation and agglomeration. However, we find that the particle size (mobility diameter) increases with increasing volumetric flow rate (see figure 4), which is in contradiction to the idea that a shorter time for growth should reduce coagulation and agglomeration. We suggest that the decrease in residence time by increasing the gas flow rate has an additional effect of increasing the cooling rate, which leads to an increase in nucleation and results in enhanced growth,

primarily by agglomeration (see figure 5(*d*)). This shows that process parameters are strongly coupled, and controlling nanoparticle nucleation and growth in a plasma process is not straightforward.

In comparison, the addition of a capillary injector does appear to reduce particle growth by coagulation and agglomeration (see figure 2). We explain how the capillary gas injector changes the residence time distribution by a simple picture of the gas flow, illustrated in figure 6. Without the capillary tube, the gas flow through the quartz tube is laminar, as indicated by the Reynolds number (see supporting information, table S1) (stacks.iop.org/JPhysD/48/314003/mmedia), and has a well-known parabolic velocity profile with a velocity maximum at the center equal to twice the average velocity. When the capillary gas injector is used, the gas flow is accelerated at the center, increasing the maximum velocity and producing a sharper velocity distribution. We note that this description assumes that the gas flow is independent of the reactive plasma. Based on this simplified picture, we suggest that the sharper flow distribution is critical to reducing the mean residence time and narrowing the residence time distribution, without affecting the cooling rate, leading to smaller and more narrowly distributed particles. It should be acknowledged, however, that the capillary injection method may lead to choking at small enough orifice diameters and/or large enough mass flow rates, which may also affect nucleation and growth. In fact, similar supersonic nozzles have been used to produce beams of metallic clusters in laser-induced metal vapor sources [29]. The coupled effects that choking may have with our atmospheric pressure, low temperature DBD system on nucleation rate, particle size, and size distribution are not clear, but are certain to be interesting and worthy of future study.

In summary, an atmospheric-pressure DBD plasma system has been studied for nanoparticle synthesis. We introduce the idea of a capillary gas injector, which is found to be critical to

controlling the residence time distribution and reducing particle size and agglomeration, which are often desired when synthesizing nanoparticles at sizes where quantum confinement and other unique physicochemical properties emerge. Future studies should focus on modeling to support our ideas and guide the design of further optimized and larger scale atmospheric-pressure plasma systems for nanoparticle synthesis.

Acknowledgments

References

[1] Spears K G 1986 *IEEE Trans. Plasma Sci.* **PS-14** 179
[2] Selwyn G S, Singh J and Bennett R S 1989 *J. Vac. Sci. Technol.* A **7** 2758
[3] Bouchoule A, Plain A, Boufendi L, Blondeau J P and Laure C 1991 *J. Appl. Phys.* **70** 1991
[4] Kortshagen U 2009 *J. Phys.* D **42** 113001
[5] Mariotti D and Sankaran R M 2010 *J. Phys. D: Appl. Phys.* **43** 323001
[6] Lopez T and Mangolini L 2014 *J. Vac. Sci. Technol.* B **32** 061802
[7] Mangolini L, Thimsen E and Kortshagen U 2005 *Nano Lett.* **5** 655
[8] Kumar A, Lin P A, Xue A, Hao B, Yap Y K and Sankaran R M 2013 *Nat. Commun.* **4** 2618
[9] Mariotti D and Sankaran R M 2011 *J. Phys.* D **44** 174203
[10] Saunders W A, Sercel P C, Lee R B, Atwater H A, Vahala K J, Flagan R C and Escorciaaparcio E J 1993 *Appl. Phys. Lett.* **63** 1549
[11] Girshick S L and Chiu C P 1989 *Plasma Chem. Plasma Process.* **9** 355
[12] Girshick S L, Chiu C P, Muno R, Cy W U, Yang I, Singh S K and Mcmurry P H 1993 *J. Aer. Sci.* **24** 367
[13] Rao N, Girshick S, Heberlein J, Mcmurry P, Jones S, Hansen D and Micheel B 1995 **15** 581
[14] Sankaran R M, Holung D, Flagan R C and Giapis K P 2005 *Nano Lett.* **5** 537
[15] Chiang W-H and Sankaran R M 2007 *Appl. Phys. Lett.* **91** 121503
[16] Lin P A and Sankaran R M 2011 *Angew. Chem. Int. Edn* **50** 1
[17] Dato A, Radmilovic V, Lee Z, Phillips J and Frenklach M 2008 *Nano Lett.* **8** 2012
[18] Sankaran R M and Giapis K P 2002 *J. Appl. Phys.* **92** 2406
[19] Shi W, Stark R H and Schoenbach K H 1999 *IEEE Trans. Plasma Sci.* **27** 16
[20] Kogelschatz U 2003 *Plasma Chem. Plasma Process.* **23** 1
[21] Nie Q Y, Cao Z, Ren C S, Wang D Z and Kong M G 2009 *New J. Phys.* **11** 115015
[22] Askari S, Macias-Montero M, Velusamy T, Maguire P, Svrcek V and Mariotti D 2015 *J. Phys. D: Appl. Phys.* **48** 314002
[23] Vons V, Creyghton Y and Schmidt-Ott A 2006 *J. Nanopart. Res.* **8** 721
[24] Torres-Gomez L A, Barreiro-Rodriguez G and Mendez-Ruiz F 1988 *Thermochim. Acta* **124** 179
[25] Lin P A, Kumar A and Sankaran R M 2012 *Plasma Process. Polym.* **9** 1184–93
[26] Mangolini L and Kortshagen U 2009 *Phys. Rev.* E **79** 026405
[27] Askari S, Levchenko I, Ostrikov K, Maguire P and Mariotti D 2014 *Appl. Phys. Lett.* **104** 163103
[28] Flagan R C and Lunden M 1995 *Mater. Sci. Eng.* A **204** 1143
[29] Dietz T G, Duncan M A, Powers D E and Smalley R E 1981 *J. Chem. Phys.* **74** 6511